ARTICLE NO. 79-0210R

Interaction of Weak Shock Waves with Screens and Honeycombs

Kwok-On Tong,* Charles J. Knight,* and B. N. Srivastava*
Avco Everett Research Laboratory, Inc., Everett, Mass.

The interaction of weak shock waves with screens and honeycombs is examined to facilitate the design of a pulsed flowing gas laser system operating at a high repetition rate. Interactions with zero and finite base flow ($M \leq 0.3$) are studied using a shock tube capable of generating weak shock waves. By reflecting the incident wave from the driven section end plate, interactions with and without base flow can be studied in a single experiment. A quasi-steady flow theory is developed to model shock interaction with screens, while a quasi-one-dimensional flow code is used for the interaction between shock waves and honeycombs. Comparisons between analytical and experimental results are made.

I. Introduction

IN high-power flowing gas laser systems, flow straightening devices such as screens and honeycombs are often used to provide the required flow uniformity in the cavity. When the laser is operated in the pulsed mode, cavity overpressure associated with energy extraction generates shock waves which propagate both upstream and downstream. Acoustic attenuators are used to weaken such waves and restore the required cavity medium uniformity before the next pulse. For a pulsed system operated at a high repetition rate (>100 pulses/s), the design of acoustic attenuators becomes more difficult due to the short time interval between pulses. In this case, the interaction of the upstream propagating shock wave with flow straightening devices becomes important to the proper design of the upstream acoustic attenuator.

The interaction of shock waves with screens and grids has been previously studied for the case of zero base flow before shock arrival.[1-3] In this paper, the interactions of weak shock waves with screens and honeycombs are studied for the cases of zero and finite base flow ($M \leq 0.3$). While the case of finite base flow is more appropriate to the pulsed laser due to the continuous flow in the system, the case with zero base flow is also included in order to assist the development of the analytical models. This range of base flow Mach numbers covers the cavity Mach number used in most blowdown and closed cycle pulsed laser systems.

A quasi-steady one-dimensional flow theory is developed to model shock interaction with screens. The screen is treated as a flow discontinuity with changes in stagnation pressure. The losses associated with the screen are based on the work of Adler[4] when the screen is not choked. When the screen is choked, the flow Mach numbers within and upstream of the screen become constants. The resultant nonlinear system of algebraic equations is then solved numerically. The interaction between weak shock waves and honeycombs is analyzed by a quasi-one-dimensional flow code. The flow within the honeycomb is assumed to be fully developed pipe flow, and the effect of discontinuous area changes at both ends of the honeycomb is also included.

In the present study, we are interested in a rectangular laser cavity configuration in which the flow, pumping, and optical directions are perpendicular to one another, with the dimensions in flow and pumping directions fractions of the optical length. Pulsed lasers are frequently operated at near ambient pressure and temperatures. However, in some cases, pressure and temperature well above and below ambient conditions have also been considered. A shock tube with a rectangular driven section is used in this study. A driver with smaller cross-sectional area than the driven section is used in conjunction with pressure burst diaphragms to generate weak shock waves. The driven section is at ambient condition initially. The acoustic attenuator being studied is placed at approximately 60 cm (2 ft) from the end of driven section. When the incident wave propagates through the attenuator, the gas in front of the wave is stationary; however, after the wave transmitted through the attenuator is reflected from the driven section end plate, it propagates against an incoming flow. Thus, in a single experiment, interactions with zero and finite base flow Mach number can be studied. Experimental results show good agreement with analytical predictions.

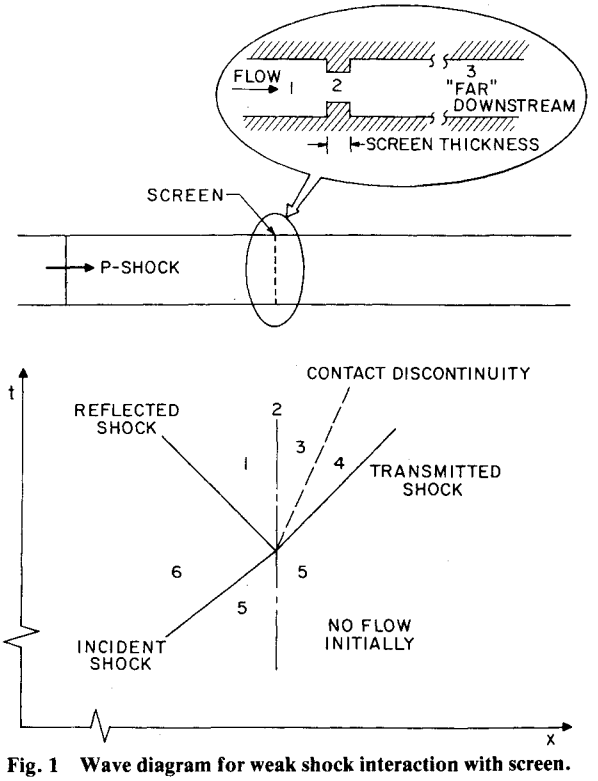

Fig. 1 Wave diagram for weak shock interaction with screen.

Presented as Paper 79-0210 at the AIAA 17th Aerospace Sciences Meeting, New Orleans, La., Jan. 15-17, 1979; submitted March 8, 1979; revision received May 12, 1980.

Index categories: Shock Waves and Detonations; Lasers.

*Principal Research Scientist. Member AIAA.

II. Screen Modeling

A screen is characterized by two primary features: 1) an area reduction followed by an increase back to the original value over a distance comparable to the wire diameter (0.005-0.025 cm), and 2) a mixing region downstream in which entropy increases over a distance of 100-200 times the mesh spacing (~2.5-5 cm). There will be frictional losses within the screen itself, but most of the stagnation pressure loss is due to pressure drag and turbulent mixing. Heat exchange between the gas and screen will be neglected. This is certainly reasonable in a steady flow situation, and it also appears reasonable in a transient flow.

It is intuitively plausible, based on the preceding discussion, to idealize the flow through the screen as depicted in the insert of Fig. 1. Steady, quasi-one-dimensional modeling will be used. Between regions 1 and 2 the flow is taken to be isentropic, and this together with the statements of mass and energy conservation lead to

$$\frac{M_1}{M_2}\left(\frac{1+\frac{\gamma-1}{2}M_2^2}{1+\frac{\gamma-1}{2}M_1^2}\right)^{\frac{1}{2}\frac{\gamma+1}{\gamma-1}}=1-s \tag{1}$$

where s is the solidity of the screen (i.e., ratio of solid area to total frontal area). Entropy increase between regions 2 and 3 can be defined by the ratio of stagnation pressures, and the analog of Eq. (1) then becomes

$$\frac{M_3}{M_2}\left(\frac{1+\frac{\gamma-1}{2}M_2^2}{1+\frac{\gamma-1}{2}M_3^2}\right)^{\frac{1}{2}\frac{\gamma+1}{\gamma-1}}=(1-s)\frac{p_{0_2}}{p_{0_3}} \tag{2}$$

Other properties downstream of the screen are related to those upstream by the following relationships:

$$\frac{T_3}{T_1}=\frac{1+\frac{\gamma-1}{2}M_1^2}{1+\frac{\gamma-1}{2}M_3^2} \tag{3a}$$

$$\frac{u_3}{u_1}=\frac{\rho_1}{\rho_3}=\frac{M_3}{M_1}\sqrt{\frac{T_3}{T_1}} \tag{3b}$$

$$\frac{p_3}{p_1}=\frac{M_1}{M_3}\sqrt{\frac{T_3}{T_1}} \tag{3c}$$

Equations (1) and (2) represent algebraic relations which can be solved for M_2 and M_3, in terms of s and M_1, once the stagnation pressure loss is defined. It will be more convenient to work here with the parameter

$$\Lambda=(p_{0_2}-p_{0_3})/sp_{0_2} \tag{4}$$

so that the right-hand side of Eq. (2) becomes $(1-s)/(1-\Lambda s)$. Note that it will always happen that $M_3<M_2\leq 1$ if $0<\Lambda<1$. Screen losses in high velocity flow were obtained by Adler[4] and reported as Fig. 4 in Ref. 5. Presumably the data can be applied to the regime of large Reynolds number based on wire diameter Re_D so that the loss should be nearly independent of Re_D. The data are replotted as solid curves in Fig. 2 vs M_2^2. For the Mach number range $0\leq M_2\leq 0.6$, Λ can be reasonably well approximated by the correlation

$$\Lambda\approx M_2^2 f(s),\quad f(s)=\begin{cases}0.83-0.9s, & 0<s<\frac{1}{2}\\ 0.38, & \frac{1}{2}<s<1\end{cases} \tag{5}$$

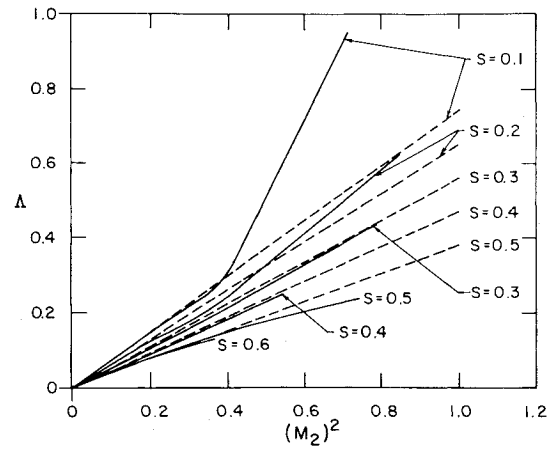

Fig. 2 Pressure losses through screens.

shown as dashed lines in Fig. 2. The range on M_2, wherein Eq. (5) is a good approximation for Λ, will be adequate for the wave strengths considered in the shock tube experiments.

Now consider an incident P-shock interacting with a screen, as shown in Fig. 1. The gas is taken to be stationary and uniform before shock arrival. The screen will be treated as a flow discontinuity, which is a valid approximation for times long enough after the interaction for the flow to be locally quasi-steady near the screen. A relevant measure of the time required to establish quasi-steady conditions is the acoustic transit time across the mixing zone downstream of the screen (e.g., 100-200 μs). Treating the screen as a flow discontinuity, the x-t diagram for the shock and screen interaction is as shown in Fig. 1. The state within the wire mesh is denoted by 2 as previously stated.

Jump relations across the various flow discontinuities in Fig. 1 lead to the following equations with $u_5=0$:

$$u_6=a_5\left(\frac{p_6}{p_5}-1\right)\Big/\gamma\sqrt{1+\frac{\gamma+1}{2\gamma}\left(\frac{p_6}{p_5}-1\right)} \tag{6a}$$

$$\rho_6=\rho_5\left(1+\frac{\gamma+1}{\gamma-1}\frac{p_6}{p_5}\right)\Big/\left(\frac{\gamma+1}{\gamma-1}+\frac{p_6}{p_5}\right) \tag{6b}$$

$$u_1=u_6-a_6\left(\frac{p_1}{p_6}-1\right)\Big/\gamma\sqrt{1+\frac{\gamma+1}{2\gamma}\left(\frac{p_1}{p_6}-1\right)} \tag{6c}$$

$$\rho_1=\rho_6\left(1+\frac{\gamma+1}{\gamma-1}\frac{p_1}{p_6}\right)\Big/\left(\frac{\gamma+1}{\gamma-1}+\frac{p_1}{p_6}\right) \tag{6d}$$

$$u_4=a_5\left(\frac{p_4}{p_5}-1\right)\Big/\gamma\sqrt{1+\frac{\gamma+1}{2\gamma}\left(\frac{p_4}{p_5}-1\right)} \tag{6e}$$

$$\rho_4=\rho_5\left(1+\frac{\gamma+1}{\gamma-1}\frac{p_4}{p_5}\right)\Big/\left(\frac{\gamma+1}{\gamma-1}+\frac{p_4}{p_5}\right) \tag{6f}$$

$$p_3=p_4 \text{ and } u_3=u_4 \tag{6g}$$

and the relations across the screen. The latter equations are given in Eqs. (1) and (2) if $M_2<1$. The flow is choked in the screen if $M_2=1$, and in that case the appropriate relations are

$$\left.\begin{aligned}&M_2=1\\ &M_1\left(\frac{2}{\gamma+1}+\frac{\gamma-1}{\gamma+1}M_1^2\right)^{-\frac{1}{2}\frac{\gamma+1}{\gamma-1}}=1-s\end{aligned}\right\}\ \text{choked flow} \tag{7}$$

The fact that $\Lambda<1$, and hence $M_3<M_2$, using the correlation given in Eq. (5) has been used in deriving the alternative in Eq.

(7). Note that when the screen is choked, another shock (and/or repetitive wave system in the flow) is likely to appear just downstream of the screen,[6] and the reflected wave from the driven section end plate will be passing through a flowfield more complicated than the simple base flow assumed here. The present model is extended to the case of $M_2 = 1$ mainly for completeness.

Reviewing Eqs. (1), (2), (6), and (7), there are evidently four unknowns, i.e., p_1/p_5, M_2, M_3, p_4/p_5, since the incident shock strength is taken to be known. The determining equations can be taken to be the two appropriate jump relations across the screen and the requirements $p_3 = p_4$ and $u_3 = u_4$. This closed nonlinear algebraic problem can be solved using Newton-Raphson iteration, and the results will be discussed in Sec. V. It is also worthwhile considering the case of very weak incident waves, in which case solution of the linearized version of the algebraic problem leads to $\Delta p_r = p_1 - p_6 = 0$ and $\Delta p_t = p_4 - p_5 = \Delta p_i$ with $\Delta p_i = p_6 - p_5$.

III. Honeycomb Modeling

A honeycomb can be considered to be an array of capillary tubes. The interaction between a shock wave and a honeycomb can thus be described by a theoretical model which accounts for the discontinuous area change at the two ends of the finite length honeycomb and an appropriate attenuation mechanism within the array of capillary tubes. The interaction of a shock wave with a discontinuous area change is modeled assuming an ideal interaction with area convergence and divergence,[7] leading to a system of waves consisting of reflected and transmitted waves. The strengths of these waves depend on the initial flow velocity within the honeycomb, effective open area, and the strength of the incident shock wave. For subsonic flow everywhere and a weak incident shock, the nature of the reflected and transmitted waves at the two ends of the honeycomb is depicted in Fig. 3. This is the wave pattern which results in our study. In general, the nature of the admissible wave patterns must be determined by the usual trial and error wave diagram procedures which can be found in the literature (e.g., Ref. 7).

There are two distinct ways in which sound could be attenuated within a finite length capillary tube: 1) dissipation by viscous and heat transfer effects; and 2) excitation and consequent acoustic energy trapping in the organ pipe modes of the capillary tube, which can be caused by impedance mismatch due to area changes at both ends of the tube. The second mechanism ultimately depends on viscosity to attenuate the acoustic energy. The present theoretical effort is directed towards modeling the response of a capillary tube with thin wall to a step input pressure pulse (i.e., a shock wave) for the cases of zero and finite base flow within the tube. Thus, only the first attenuation mechanism is considered because the impedance mismatch due to area changes is considered to be small. For a typical pulsed laser system, a capillary tube with base flow is more relevant due to continuous gas flow within the system; however, in order to develop an understanding of the relevant physics by comparison of the proposed analytical model with experimental results, we have also included the case of zero base flow.

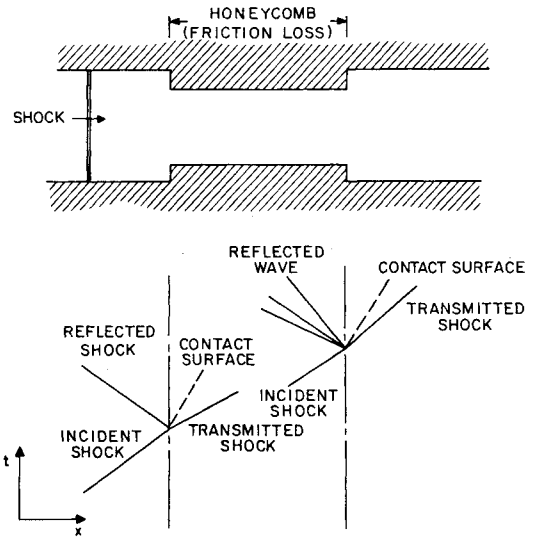

Fig. 3 Wave diagram for weak shock interaction with honeycomb.

A quasi-one-dimensional flow modeling is used to treat the interaction and subsequent decay of a step input pressure pulse to a capillary tube. The basic governing equations that describe the unsteady, one-dimensional flow of a gas in a duct are

Conservation of mass:

$$\frac{\partial}{\partial t}(\rho A) + \frac{\partial}{\partial x}(\rho A u) = m_1 \tag{8a}$$

Conservation of momentum:

$$\frac{\partial}{\partial t}(\rho u A) + \frac{\partial}{\partial x}(\rho u^2 A) + \frac{\partial p}{\partial x} A = m_2 \tag{8b}$$

Conservation of energy:

$$\frac{\partial}{\partial t}(\rho A e) + \frac{\partial}{\partial x}(\rho A u e) + p\frac{\partial}{\partial x}(uA) = m_3 \tag{8c}$$

where A is the cross-sectional area of the duct; e is the internal energy of the gas; and m_1, m_2, and m_3 represent the source-sink terms with units of mass, momentum, and energy flux per unit length of the duct, respectively. In addition to Eqs. (8), we have the ideal equation of state

$$p = \rho RT \tag{9}$$

and

$$e = RT/(\gamma - 1) \tag{10}$$

where R is the gas constant and γ is the ratio of specific heats.

The basic analytical modeling consists of appropriate representation of source-sink terms m_1, m_2, and m_3. At flow velocities of current interest, the heat transfer effects can be neglected. However, the viscous effects representative of terms m_1, m_2, and m_3 in Eqs. (8) need to be modeled. There are several considerations that determine the nature of these viscous terms, i.e., the thickness of the boundary layer as compared to the capillary tube, and the nature of the flow (laminar or turbulent) within the capillary tube. For present purposes, a viscous model that assumes a fully developed pipe flow (leading to a friction factor concept) is adopted. For this case, the source terms are

$$m_1 = 0 \tag{11a}$$

$$m_2 = -DA \tag{11b}$$

$$m_3 = ADu \tag{11c}$$

where D represents the drag force per unit volume. The expression for D is given as[8]

$$D = (\lambda/2d)\rho u|u| \tag{12}$$

where λ is the resistance coefficient, and d is the hydraulic diameter. The resistance coefficients for fully developed laminar and turbulent flow are given as[9]

$$\lambda = 64/R \text{ laminar flow } 0 < R < 3 \times 10^3 \tag{13a}$$

$$\lambda = 0.3164/R^{1/4} \text{ turbulent flow } 3 \times 10^3 < R < 10^5 \tag{13b}$$

where R is the Reynolds number based on the local core flow and is defined as $R=ud/\nu$. The viscous terms represented by Eqs. (11) are not most general in nature. In particular, if the boundary layer within the capillary tube is very small compared to the tube radius, Eqs. (11) will underestimate the attenuation.

A time-dependent solution of Eqs. (8-10) with m_1, m_2, and m_3 represented by Eqs. (11) is sought. Such a solution is generated by a numerical scheme that utilizes a fixed piecewise uniformly spaced Eulerian grid system. The flow discontinuities are allowed to "float" through the fixed Eulerian grid. The boundary and discontinuity flow properties are updated to the current time level using a local characteristic update scheme. Away from flow discontinuities, a second-order accurate MacCormack predictor-corrector scheme is used to advance flow information at Eulerian grid points in time. A characteristic update scheme is needed at grid points where source-sink terms in Eqs. (8) are discontinuous. A nonconstant grid spacing is used to save computational time. (For further details of the numerical scheme, one is referred to Ref. 10.)

IV. Experimental Apparatus

In the present study, we are mainly concerned with weak shock waves having shock Mach numbers between 1.0 and 1.2. With $\gamma=1.4$, the corresponding pressure ratio ranges from 1.0-1.51. The required pressure ratio across the diaphragm for generating such a range of weak shock waves in a constant area shock tube is less than 2.5. With such a small pressure difference across the diaphragm, it appears difficult to find appropriate diaphragm materials for sufficient control of the incident shock strength. One way to increase the pressure difference across the diaphragm is to use a driver with smaller cross-sectional area than the driven section. The performance of a shock tube with area change near the diaphragm has been studied by Russell.[11] Following the wave systems suggested in Ref. 11, the performance of shock tubes with different driver and driven sections has been calculated. Figure 4 shows the required pressure ratio across the diaphragm for the case of $A_1/A_4=5.7$, where A_1 an A_4 are the cross-sectional area for the driven section and driver, respectively. The required pressure ratio across the diaphragm for a constant area shock tube is also shown in Fig. 4 for comparison. Several diaphragm materials have been tested using a 3.8 cm (1½ in.) diam stainless steel tube as the high pressure section, and the range of bursting pressure ratios is also shown on the right-hand side of Fig. 4. It appears that sufficient control of the strength of incident shock wave can be achieved with these diaphragm materials for the case of $A_1/A_4=5.7$.

Figure 5 is the schematic of the shock tube. The driver section is composed of two sections of 3.8 cm (1½ in.)-i.d. stainless steel tube with a total length of 3 m (10 ft). Pressure in the driver section is monitored by a pressure gage. The driven section has an internal dimension of 4.4 cm × 14.6 cm (1¾ in. × 5¾ in.) which gives $A_1/A_4=5.7$. The transition from circular to rectangular takes place abruptly at the diaphragm location, and thus the transition section is eliminated. The driven section consists of four components. The first 3-m (10-ft)-long section is made with a 0.32 cm (⅛ in.) thick aluminum rectangular tube stiffened with aluminum plates. The two 61 cm (2 ft) sections and the 30.5 cm (1 ft) long test section are all made out of 1.9-cm (¾ in.)-thick aluminum plates. The test section is located between the two 61-cm sections and houses the honeycomb. The study on screens was carried out without the test section, and the screen was clamped between the 61-cm sections. Kistler pressure transducers are located in both 61-cm sections so that the pressure on both sides of the screen and honeycomb can be measured. Another Kistler pressure transducer is located in the first 61-cm section for triggering. Thin film heat transfer gages with nominal 500-Ω resistance are also used for measuring shock speed. Windows of 11.4 and 3.8 cm (4½ and 1½ in.) diam are provided in the 61-cm sections for taking

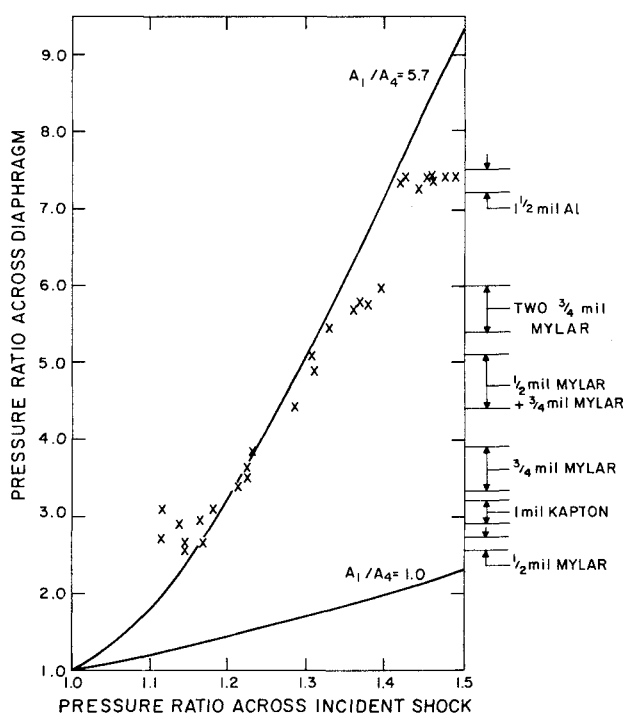

Fig. 4 Performance of shock tube with pressure-burst diaphragm.

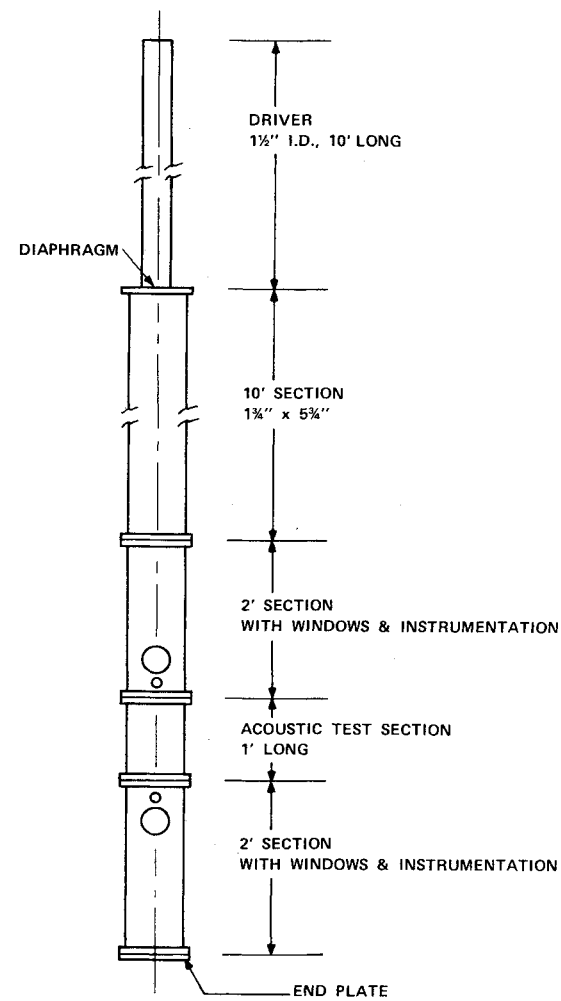

Fig. 5 Schematic of shock tube.

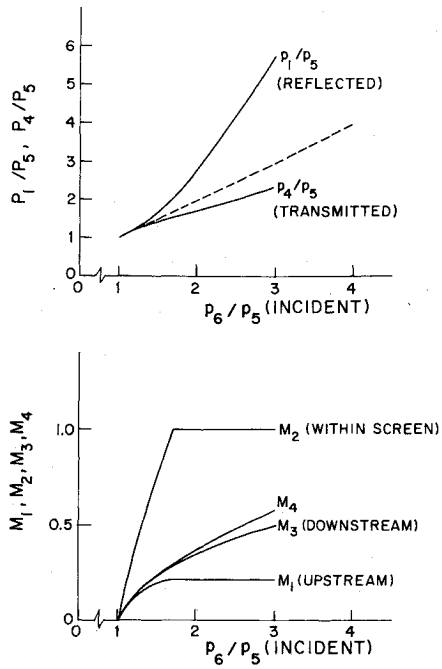

Fig. 6 Interaction between shock wave and 200 mesh screen with zero base flow. (Refer to Fig. 1 for the designation of different flow regions.)

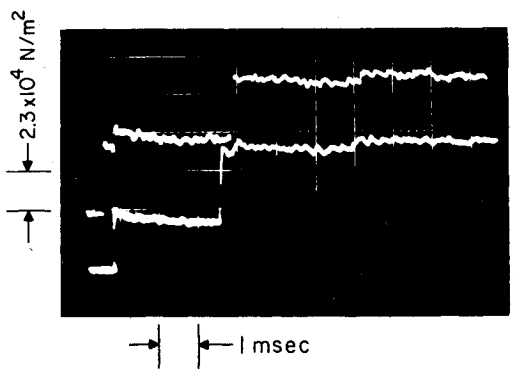

Fig. 7 Pressure traces with 200 mesh screen.

shadowgraph and Schlieren pictures. Pressure ratio across the incident shock at various diaphragm loadings is also shown in Fig. 4. The data show good agreement with predicted performance.

When the incident shock propagates into the screen and honeycomb, the gas in front of the shock wave is stationary; after the shock wave is reflected from the end plate of the driven section, it propagates against an incoming flow. Therefore, in a single experiment, the interaction between shock wave and screen (honeycomb) can be studied for the cases of zero and finite base flow in the screen (honeycomb) simultaneously. In the present study, a solid driven section and end plate was used.

For the study of interaction between weak shock wave and screens, 32 and 200 mesh screens have been used. The solidities of the screens are 0.58 and 0.64, respectively. The pressure drop coefficients ($2\ \Delta p/\rho u^2$) of the screens, as measured in a low-speed wind tunnel ($u \approx 11$ m/s), are 1.9 and 4.2, respectively. Each screen was pulled tight during the installation and no significant sagging was observed after several runs.

For the study on shock interaction with honeycomb, aluminum honeycomb with a cell size of nominal 0.48 cm (3/16 in.) and a 0.0018 cm (0.0007 in.) thick wall was used. The open area ratio of such a honeycomb is 99%. Both 10.2 and 30.5-cm (4 and 12-in.) thick pieces have been tested. Since the available honeycomb was only 10.2 cm thick, the 30.5 cm thick piece was made up by three pieces of 10.2 cm thick honeycomb. These three pieces were carefully matched so that over 95% of the cells were continuous cells over the entire thickness of the honeycomb.

V. Results and Comparisons

Screen

The flow model described in Sec. II has been used to predict the interaction between weak shock wave and screen for the case of zero base flow. Figure 6 shows the result for the 200 mesh screen (solidity = 0.64). In this case, the reflected wave is always a shock wave. The flow Mach number upstream of the screen remains constant for $M_2 = 1$. Because the flow velocity is continuous across the contact surface, the impedance ratio across the contact discontinuity is defined by the Mach number ratio. For the 200 mesh screen, this impedance ratio is nearly one, especially for weak incident waves.

Figure 7 gives the pressure traces at both sides of the 200 mesh screen. The upper and lower traces are outputs from the upstream and downstream transducers, respectively. The

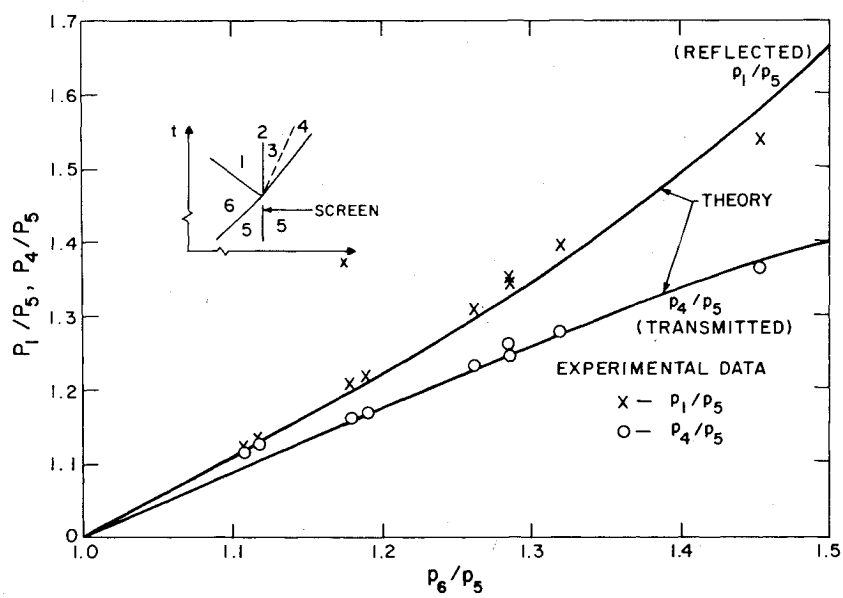

Fig. 8 Shock interaction with 200 mesh screen (zero base flow).

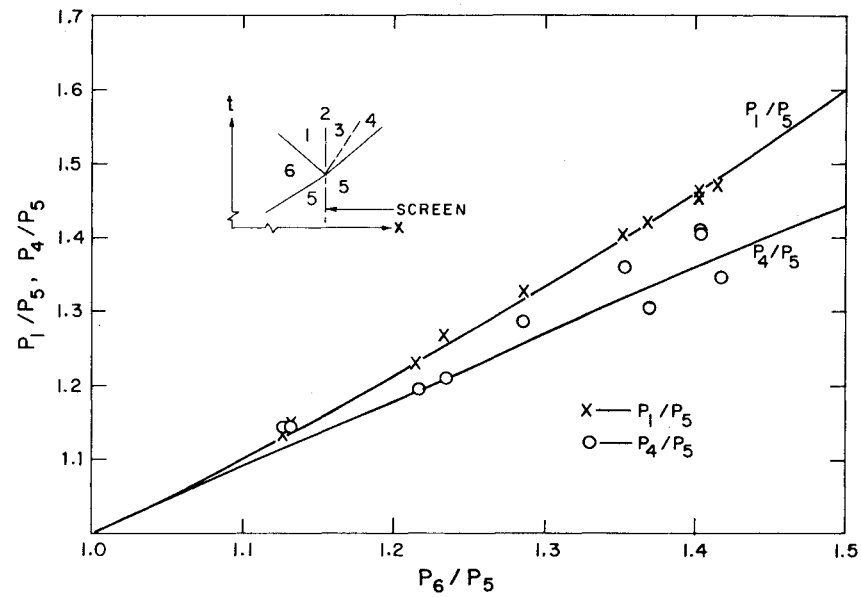

Fig. 9 Shock interaction with 32 mesh screen (zero base flow).

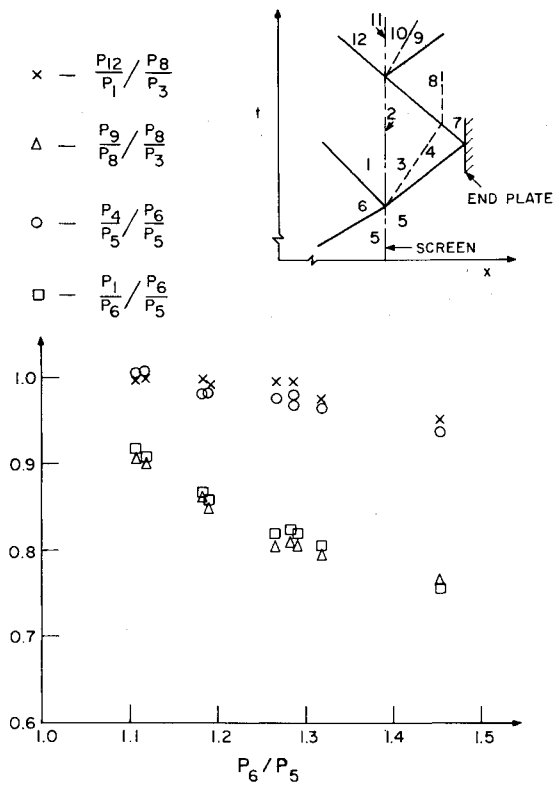

Fig. 10 Shock interaction with 200 mesh screen (finite base flow).

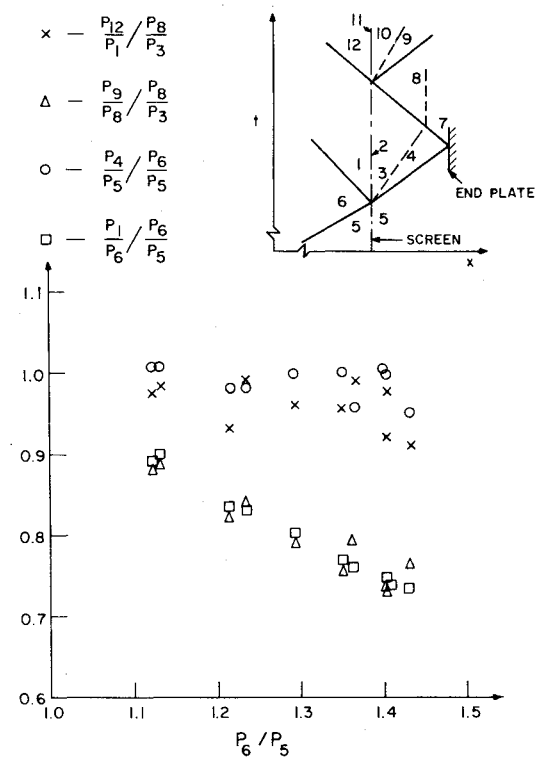

Fig. 11 Shock interaction with 32 mesh screen (finite base flow).

results for zero base flow are summarized in Fig. 8. Here, the measured pressure levels behind the transmitted wave and the reflected wave from the screen are shown for different incident shock strengths. The prediction previously shown on Fig. 6 is also included for comparison. The agreement between data and predictions is good. Similar results are shown in Fig. 9 for the case of the 32 mesh screen (solidity = 0.58). Although the scatter in experimental data is larger than in the case of the 200 mesh screen, the agreement between experimental results and analytical predictions is still reasonable.

Figures 10 and 11 show the experimental results for interaction of a shock wave with the 200 and 32 mesh screens, respectively, for the case of finite base flow. Here, the transmission and reflection of the shock wave by the screen are shown for various incident shock strengths. The transmission and reflection of the incident shock (i.e., the case of zero flow) are also included for comparison. Again, the experimental data for the 32 mesh screen shows larger scatter than for the 200 mesh screen. Even with such scatter, the data indicate that for the cases studied, the effect of base flow on shock wave attenuation is not significant.

Honeycomb

Figure 12 shows the outputs from the pressure transducers located at both ends of the 30.5 cm long honeycomb. Here, the upper trace is for the transducer upstream of the honeycomb, and the lower trace is for the downstream transducer. In this particular case, the pressure ratio across the

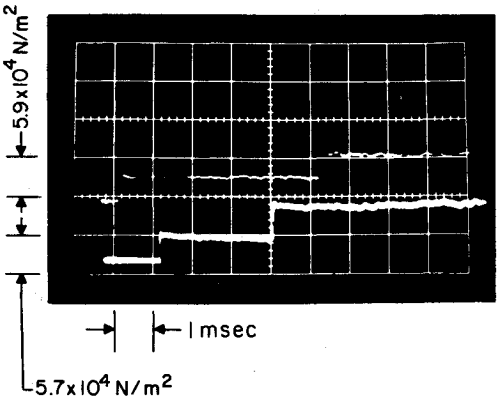

Fig. 12 Pressure traces with 30.5 cm honeycomb.

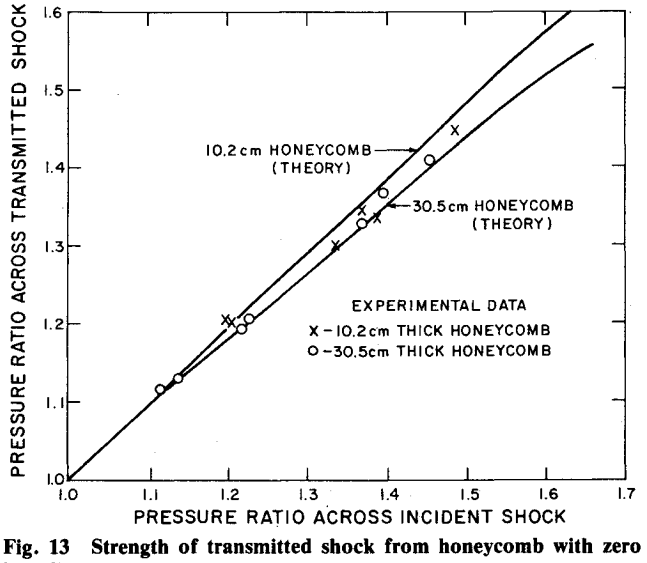

Fig. 13 Strength of transmitted shock from honeycomb with zero base flow.

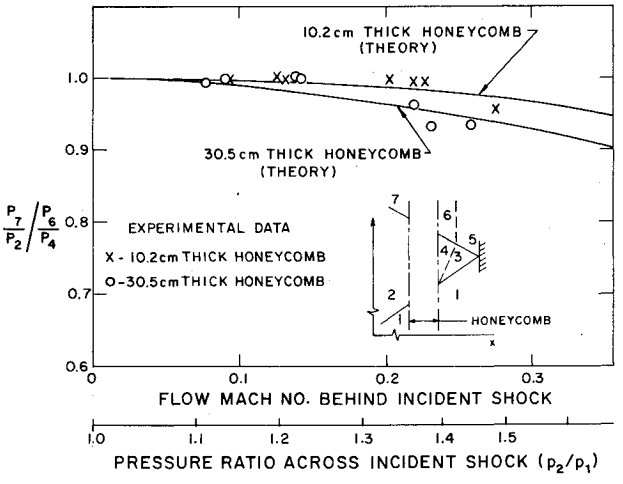

Fig. 14 Shock interaction with honeycomb (finite base flow).

incident shock wave was 1.4. The reflection of incident shock wave caused by the discontinuous area change at the upstream end of the honeycomb is not evident. This is because the honeycomb used has a very small area blockage (99% open), and thus the reflected wave from the upstream end of the honeycomb is very weak.

Figure 13 summarizes the experimental data for the case of zero base flow. It should be mentioned that both 10.2 cm and 30.5-cm honeycombs were housed in the 30.5 cm test section, and the transducers were located at fixed distances from the ends of the 30.5-cm section. Thus, in the 10.2-cm honeycomb experiments, the transducers were located at 15.9 cm (6¼ in.) from each end of the honeycomb, while in the 30.5-cm honeycomb experiments, the distance was 5.7 cm (2¼ in.). The analytical predictions given by the one-dimensional flow code (Sec. III) are also included. These predictions are based on the assumption that fully developed pipe flow exists along the entire length of the honeycomb. The agreement between the experimental data and analytical predictions is good for the case of the 30.5 cm long honeycomb. However, for the case of the 10.2 cm honeycomb, the code gives a slightly stronger transmitted wave. This may be due to the fact that fully developed pipe flow has not been established in the 10.2 cm honeycomb. Thinner boundary layers would lead to higher wall shear stress, and hence attenuation, than predicted with Eqs. (13).

Figure 14 shows the experimental results for the case of finite base flow in the honeycomb. Both the pressure ratio across the incident shock and the flow Mach number behind the incident shock are shown as the abscissa in Fig. 14, and the ordinate gives the variation in pressure ratio across the reflected shock at both ends of the honeycomb. The predictions given by the one-dimensional flow code are also shown in Fig. 14. Since the entire flowfield is generated by the incident shock, an infinitesimal weak incident shock will generate a base flow of zero Mach number and an infinitesimally weak reflected wave. Thus, when the base flow Mach number approaches zero, the pressure ratio across the reflected transmitted wave remains unchanged at both ends of the honeycomb. Even with the scatter in the experimental data, the agreement between predictions and experiment results is generally good. Again, the agreement is better in the case of the 30.5 cm long honeycomb.

VI. Conclusions

A shock tube study was carried out for the interaction of weak shock waves with screens and honeycombs. Incident shock waves with pressure ratio ranging from 1.1 to 1.5 were generated by pressure-burst diaphragms. Using a solid driven section end plate to reflect the incident shock wave, interactions with and without base flow were studied simultaneously in a single experiment.

A quasi-steady one-dimensional flow theory was developed to model shock wave interaction with screens for the case of zero base flow. The screen was treated as a flow discontinuity with changes in stagnation pressure. Screens with 32 and 200 meshes were used in the shock tube experiment. Measured strengths of the transmitted and reflected waves show good agreement with predictions. For the case of finite base flow ($M \leq 0.3$), experimental data indicate that for the cases studied, the effect of base flow is not significant.

In analyzing the interaction between weak shock waves and honeycombs, a quasi-one-dimensional flow code was used in the cases of zero and finite base flow. Flow inside the entire honeycomb was assumed to be fully developed, and the effect of area discontinuities at both ends of the honeycomb was also included. Honeycombs 10.2 and 30.5 cm (4 and 12 in.) long with 0.48-cm (3/16 in.) cell size and 99% open were used in the shock tube experiment. Both experimental data and analytical prediction show that for the cases studied, changes in shock strength across the entire honeycomb are less than 10%.

Acknowledgments

The authors wish to express their thanks to Dr. P. I. Singh for many helpful discussions. This work is funded under DARPA/MIRADCOM Contract DAAK-40-78-C-0126.

References

[1] Bowman, J. E. and Niblett, G.B.F., "The Passage of a Plane Shock Wave through a Wire Gauze," *Proceedings of the Physical Society*, London, England, 1955, Sec. B, Vol. 68, Dec. 1955, pp. 1008-1016.

[2] Dosanjh, D. S., "Interaction of Grids with Traveling Shock Waves," NACA Tech. Note 3680, 1956.

[3] Franks, W. J., "Interaction of a Shock Wave with a Wire Screen," Institute of Aerophysics, University of Toronto, Canada, UTIA Tech. Note No. 13, May 1957.

[4] Adler, A. A., "Variations with Mach Number of Static and Total Pressures through Various Screens," NACA Wartime Report L-23 (Originally Confidential Bulletin L5F-28, 1946).

[5] Cornell, W. G., "Losses in Flow Normal to Plane Screens," *Transactions of the American Society of Mechanical Engineers*, Vol. 80, No. 4, May 1958, pp. 791-799.

[6] Dosanjh, D. S., "Some Comments on a Theoretical and Experimental Study of Shock Tube Flows," *Journal of the Aeronautical Sciences*, Vol. 22, Nov. 1955, pp. 797-799.

[7] Rudinger, G., *Nonsteady Duct Flow*, Dover, New York, 1969.

[8] Schlichting, H., *Boundary-Layer Theory*, McGraw-Hill, New York, 1968.

[9] Davis, J. T., *Turbulence Phenomena*, Academic Press, New York, 1972.

[10] Srivastava, B. N., Knight, C. J., and Zappa, O., "Acoustic Suppression in a Pulsed Laser System," *AIAA Journal*, Vol. 18, May 1980, pp. 555-562.

[11] Russell, D. A., "A Study of Area Change near the Diaphragm of a Shock Tube," California Institute of Technology, Pasadena, Calif., GALCIT Hypersonic Research Project Memo No. 57, July 1960.